Inner-space reconstruction of quasicrystal structure factors

Marko Vukobrat Jarić
Department of Physics, Texas A&M University, College Station, Texas 77843
and Nikola Tesla University, Knin, Republic of Serbian Krayina

Shi-Yue Qiu
Department of Physics, Iowa State University, Ames, Iowa 50011
(Received 27 July 1993)

An inner-space approach to the structure-factor reconstruction in quasiperiodic crystals is presented. This approach is based on the representation of a quasiperiodic crystal as a higher dimensional periodic crystal (hypercrystal) whose hyperatom form factors can often be expressed as continuous functions of the inner-space components of the scattering wave vector. Thus, the reconstruction of the structure factors is reduced to a convenient parametrization of these functions (exemplified here by a Taylor series expansion) with the parameters to be determined through a fit of the experimentally measured diffraction intensities. The fitting parameters may also include locations of the hyperatoms, their chemical composition, and Debye-Waller factors. As an illustration, we applied this technique to reconstruct neutron scattering structure factors of icosahedral quasicrystal i-$Al_{0.570}Cu_{0.108}Li_{0.322}$. We found consistent results with these obtained earlier using a method based on periodic approximants of quasiperiodic crystals.

I. INTRODUCTION

The determination of atomic structures is still one of the most fundamental open problems in the quasicrystal field and much of the recent research efforts have been devoted to developing various approaches for its solution. A solution of this problem may be broken into several steps. One could begin by reconstructing the quasicrystal structure factors from the experimentally measured diffraction intensities. Next, by calculating the inverse Fourier transform of the reconstructed structure factors, one would determine and analyze an approximate thermally averaged quasicrystal scatterer density. Then, based upon the density analysis, one could model the ideal quasicrystal structure and fluctuations around it. Finally, one should provide a physical interpretation of the obtained structure model, for example, in terms of its building blocks and principles of their packing. Many investigations of quasicrystals start from the assumption that they can be idealized by *quasiperiodic* crystals and, thus, can be represented by higher dimensional *periodic* crystals (hypercrystals).[1–5] We shall also adopt this view in the present paper and use the terms quasicrystal and quasiperiodic crystal interchangeably.[6] Then, the first three steps of quasicrystal structure determination can be carried out, and are indeed often simpler, on the associated hypercrystal. In this paper, we shall continue our earlier work on general structure-factor reconstruction methods for quasicrystals.[7] However, we shall formulate and use here another, complementary, general method that starts from a similar idea to the ones developed independently and differently by others.[8,9] Like in Ref. 7, we shall illustrate our reconstruction method on the icosahedral quasicrystal i-$Al_{0.570}Cu_{0.108}Li_{0.322}$. However, we are not focusing here on the structure determination of i-$Al_{0.570}Cu_{0.108}Li_{0.322}$ *per se*, and we shall report elsewhere on the density analysis[10] and modeling[11] of this quasicrystal.

The structure of a solid can often be represented by $\rho(\mathbf{r})$, thermally averaged density of scatterers, which can be reconstructed from the structure factors $F_{\mathbf{Q}}$ by the inverse Fourier transform,

$$\rho(\mathbf{r}) = \sum_{\mathbf{Q}} F_{\mathbf{Q}} e^{-i\mathbf{Q}\cdot\mathbf{r}}, \tag{1.1}$$

where the sum is over the reciprocal lattice vectors $\mathbf{Q}$. The structure factor is generally a complex number, having an amplitude and a phase, $F_{\mathbf{Q}} = |F_{\mathbf{Q}}|e^{i\theta(\mathbf{Q})}$. However, a diffraction experiment measures the Bragg peak intensities $I_{\mathbf{Q}}$, providing only the amplitudes of the structure factors, $|F_{\mathbf{Q}}| = s\sqrt{I_{\mathbf{Q}}}$, but not their phases. Moreover, the proportionality constant $s > 0$ is often experimentally undetermined. A partial phase information can be obtained using the contrast variation method which is a standard tool for periodic crystals and also applicable to quasiperiodic crystals.[12–14] For periodic crystals, the complete reconstruction of the phase information from the diffraction data can be accomplished using the Hauptman-Karle method.[15,16] Unfortunately, this method is not applicable to general quasiperiodic crystals and alternative approaches have to be used. Although a method of comparable generality is not yet known for quasicrystals, a method was recently developed for a class of quasiperiodic crystals for which structures of *periodic* crystals approximating them are known.[7] This method has been successfully applied to the icosahedral quasicrystal i-$Al_{0.570}Cu_{0.108}Li_{0.322}$.[7] Since periodic approximants are not known for some quasicrystals, we shall present in this paper another method which does not rely

on the existence or knowledge of the approximants.

The method which we shall present is based on a representation of a quasiperiodic crystal by a higher dimensional periodic crystal (hypercrystal) that is built out of hyperatoms, extended objects of codimension 3. (A reader who is not quite fluent with the hypercrystal approach to quasiperiodic crystals may find it useful to consult the Appendix.) Therefore, the structure factor can be written as a product of the hyperlattice structure factor times the sum of the hyperatom factors within a unit cell of the hypercrystal. Although highly irregular functions of the physical scattering wave vector alone, the hyperatomic form factors can often be expressed as continuous functions of the physical scattering wave vector *and* its orthogonal complement in the hyperspace. For the sake of motivation, let us consider an Ammann icosahedral tiling with point scatterers located at its vertices.[5] The associated hypercrystal is a six-dimensional simple hypercubic lattice with a single hyperatom, an inner space rhombic triacontahedron, per unit cell. Its structure factor, expressed as a function of the inner-space wave vector, is simply the inner-space Fourier transform of the triacontahedron. Indeed, while the structure factor is a pathological function of the physical scattering wave vector shown in Fig. 1(a), it is a simple, continuous function of the inner-space wave vector shown in Fig. 1(b). The small scatter away from a continuous function, which can be noticed in the figure, is due to the fact that although approximately spherical, the triacontahedron has only the icosahedral symmetry, so that its Fourier transform depends not only on the magnitude of the wave vector $\mathbf{Q}^{\perp}$, but also on its direction.

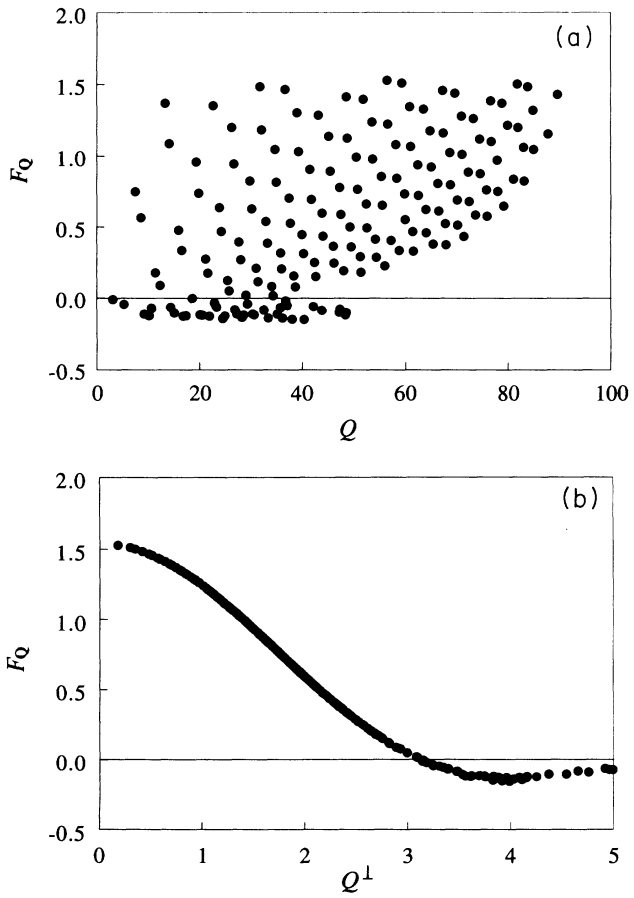

FIG. 1. The exact structure factor of the Ammann tiling plotted as a function of the physical (a) and the inner-space (b) scattering wave vectors for the six Miller indices ranging between -2 and 2.

The above observation for the Ammann quasicrystal has been transplanted literally to several real, centrosymmetric icosahedral quasicrystals.[8,17] Their (partial) scattering intensities were plotted as functions of the magnitude of the inner-space wave vectors and the nodes where the structure factors should change the sign were estimated. However, as pointed out in these works, in addition to its obvious limitation to centrosymmetric quasiperiodic crystals (for which the phase factors are ± 1), such a simple approach may run into both technical and conceptual difficulties with more general quasicrystals. The main reason is that rather than falling on a simple curve, the intensity data plotted as a function of $Q^{\perp}$ may be generally quite scattered. As a case in point, we show in Fig. 2(a) the neutron scattering data[18] for the icosahedral quasicrystal i-$Al_{0.570}Cu_{0.108}Li_{0.322}$. Whereas looking at the data in Fig. 2(a) one could reasonably argue that there is a node near $Q^{\perp}=0.7$ Å^{-1}, because of the large scatter of the data it would be hard to pinpoint the node accurately. On the other hand it would be much less convincing to argue either for the presence or the absence of the nodes at the smaller values of $Q^{\perp}$, for example, between 0.3 and 0.4 Å^{-1}.

In addition to the data scatter caused by the lack of spherical symmetry already mentioned above, there are obviously also the unavoidable random experimental errors. However, there may be also more systematic sources of the data scatter. In fact, since Q is a highly irregular function of $Q^{\perp}$, as illustrated in Fig. 3 for a simple icosahedral lattice, any continuous dependence of the diffraction intensity on Q would show up as an irregular $Q^{\perp}$ dependence. For example, in case of x-ray diffraction, there is a (weak) Q dependence of the atomic form factors. The associated data scatter could be only partially reduced by an appropriate average correction factor. Similarly, the thermal fluctuations of the atoms are manifested in a Gaussian (Debye-Waller) Q dependence of the diffraction intensities which would also cause a data scatter. Indeed, as shown in Fig. 2(b), if the data are corrected for an average thermal Debye-Waller factor (taken from Ref. 7), the node near $Q^{\perp}=0.7$ Å^{-1} becomes slightly more apparent.

It is more difficult to eliminate the Q dependence caused by the presence of more than one hyperatom per unit cell of the hypercrystal. Not only will different hyperatoms generally have different atomic form factors and the thermal Debye-Waller factors, so that the aforementioned average corrections will be only approximate, but a Q dependence, and the accompanied data scatter, will also be introduced through the phase factors associated with the positions of the hyperatoms within the unit hypercell. This can be clearly seen in Fig. 2(b), where most of the data scatter remains even after the Debye-Waller correction. In fact, a careful examination

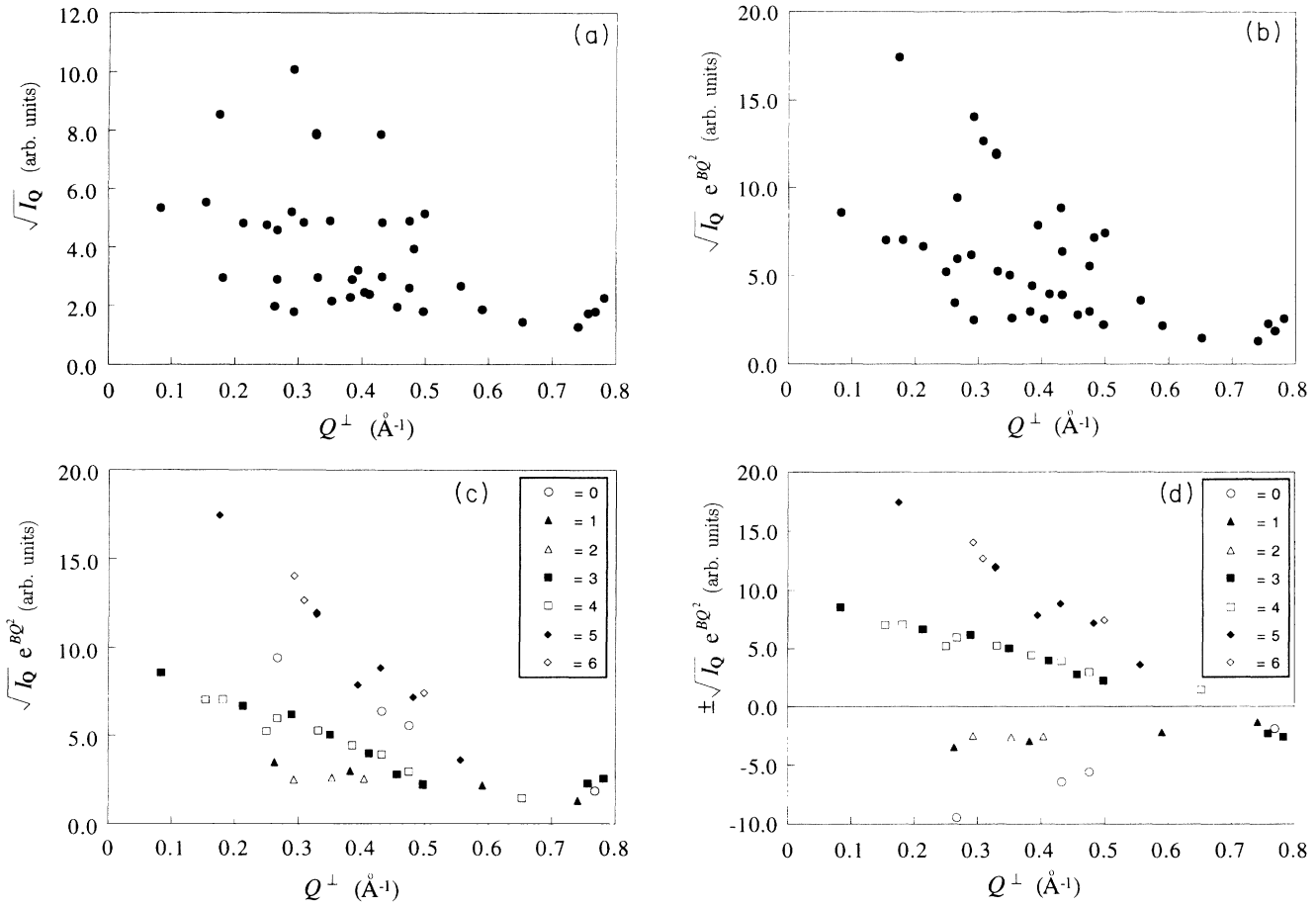

FIG. 2. (a) Square root of the diffraction intensity measured for i-$Al_{0.570}Cu_{0.108}Li_{0.322}$ (Ref. 18) is plotted as a function of the inner-space scattering wave vector. (b) The same data as in (a) but corrected for an overall thermal Debye-Waller factor with $B = 0.012$ Å^2 (Ref. 7). (c) The same data as in (b) but with the data corresponding to different branches identified by different symbols, as explained in the text. (d) The same data as in (c) but including the signs (phase factors) calculated in Ref. 7.

reveals a "branching" of the data with a relatively small scatter of data in each branch. Precisely such branching, which can be easily separated from the one caused by the "intrinsic" branching of the $Q^{\perp}$ vs Q dependence seen in Fig. 3, is a manifestation of the presence of multiple hyperatoms in the unit cell of the hypercrystal. As will be explained below, we show in Figs. 2(c) and 2(d) that the branching in Fig. 2(b) is consistent with the assumption that the structure of the hypercrystal is of the form VE_6B, with one hyperatom at the vertex, one at each of the six edge centers, and one at the body center of the six-dimensional hypercubic unit cell.

In order to deal with the data scatter, it has been suggested that a quantitative estimate for the node locations could be obtained by approximating the hyperatoms, to lowest order, with spheres[8] or ellipsoids[18] placed at the locations determined using other considerations, such as hypercrystal Patterson functions.[19] This approach can be justified when the diffraction data set is so small that it *alone* might not be sufficient to determine the shapes of hyperatoms more precisely. However, as a *de facto* structure modeling, this approach generally leads to too

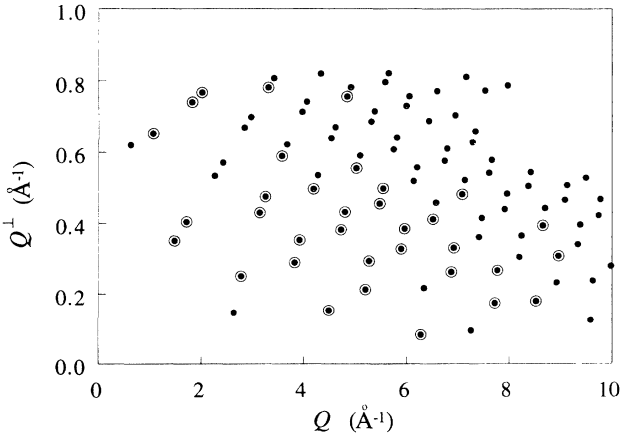

FIG. 3. Inner-space components of the reciprocal hyperlattice vectors are plotted as a function of the physical space components. The same Miller indices as in Fig. 1 are used and the points with experimentally measured i-$Al_{0.570}Cu_{0.108}Li_{0.322}$ intensities shown in Fig. 2 are circled.

short interatomic separations, too large voids, or other unphysical aspects of the resulting structure, thus requiring more detailed and *explicit* modeling.[18]

In order to separate as much as possible structure-factor reconstruction from an actual structure modeling, our philosophy is to first reconstruct the phases of the structure factors directly in the reciprocal hyperspace. In other words, rather than to model hyperatom shapes using an insufficient diffraction data set, we approximate their Fourier transforms, the inner-space atomic form factors. A systematic approximation can be made by a truncated expansion of the form factors with respect to an appropriate basis, such as, symmetry adjusted spherical harmonics, Hermite functions, etc. In cases when the hyperatoms are considerably extended in the inner-space directions, their form factors are correspondingly localized and can be well approximated by a Taylor series with respect to the inner-space scattering wave vector. Then, the expansion coefficients can be determined, and the quasicrystal structure factors reconstructed, through a fit of the experimentally measured diffraction intensities. More generally, the fitting parameters may also include locations of the hyperatoms, their chemical composition, and Debye-Waller factors.

As an illustration, we shall use this method to reconstruct neutron scattering structure factors of icosahedral quasicrystal i-$Al_{0.570}Cu_{0.108}Li_{0.322}$. The structure factors that we shall obtain are consistent, as evident in Fig. 4, with our earlier structure-factor reconstruction which used a different method based on periodic approximants of quasiperiodic crystals.[7] The absolute scales determined by the two methods are within the error bars of each order, and the determined phases are identical except for two very weak peaks.

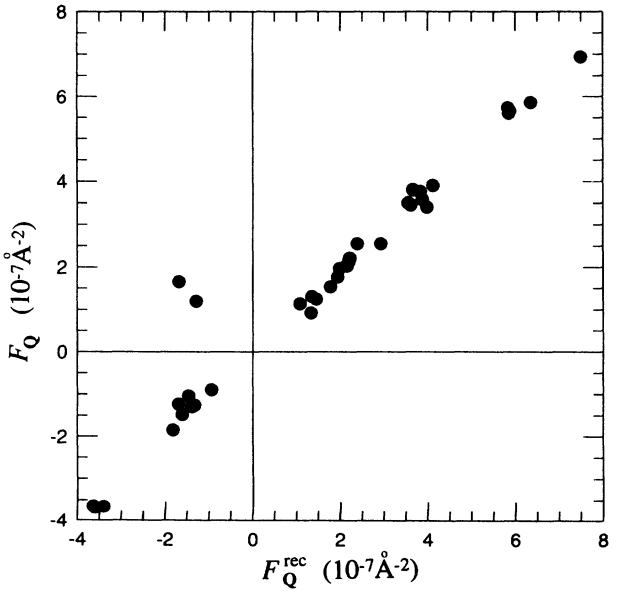

FIG. 4. The scatter graph of the approximate (parametrized) structure factors calculated here vs the structure factors reconstructed in Ref. 7 using the method of rational approximants.

Once the structure factors are reconstructed, the associated quasiperiodic density can be calculated by the inverse Fourier transform. Moreover, with the fitting parameters determined, the approximate form factor of each hyperatom can be written analytically and, thus, interpolated values for unobserved peaks can be calculated, leading to more accurate reconstructed densities of individual hyperatoms. Although a structure modeling, such as the one for i-$Al_{0.570}Cu_{0.108}Li_{0.322}$ which we will present elsewhere,[11] must rely on some additional information and considerations, an analysis of the reconstructed density can be used as an excellent *guide*.[10]

We shall assume in the rest of the paper that the reader is thoroughly acquainted with the basic notions about quasiperiodic crystals summarized in the Appendix. For the sake of completeness and in order to establish the notation, we derive there a general expression for the quasicrystal structure factor as a sum of the Fourier transforms of the hyperatoms in the unit cell of the associated hypercrystals. In Sec. II we discuss the parameters needed to describe the structure factors and, in particular, the Taylor expansion of the inner-space form factors. It is shown how these parameters and the expansion coefficients can be determined by fitting the experimentally measured diffraction intensities. Then, in Sec. III, we illustrate our method by reconstructing the neutron scattering structure factors of the icosahedral quasicrystal i-$Al_{0.570}Cu_{0.108}Li_{0.322}$ using the published neutron diffraction data.[18] The results are discussed in Sec. IV and the conclusions presented in Sec. V.

II. STRUCTURE-FACTOR EXPANSION

The objective of quasiperiodic crystal structure modeling is to determine the locations of the hyperatoms ($\bar{\mathbf{r}}_\mu$), their chemical compositions ($p_{\mu i}$), shapes ($\mathbf{s}_\mu$ *and* $v_\mu^\perp$), and Debye-Waller factors ($e^{-\mathbf{Q}\cdot\bar{\mathbf{B}}_\mu\cdot\mathbf{Q}}$). In principle, the unknown parameters can be obtained by a brute-force fit of the experimentally observed diffraction intensities $I_{\mathbf{Q}}$, for example, by the weighted least-squares optimization

$$\min \sum_{\mathbf{Q}} \frac{\left(I_{\mathbf{Q}} - |\frac{1}{s}F_{\mathbf{Q}}|^2\right)^2}{\sigma_{\mathbf{Q}}^2}, \tag{2.1}$$

where $\sigma_{\mathbf{Q}}$ is the experimental error for measuring $I_{\mathbf{Q}}$. The greatest difficulty in such a brute-force approach present the hyperatom shapes whose modeling requires, *a priori*, an infinite number of parameters.

It is often possible to determine the number and the locations of hyperatoms in the unit hypercell by studying Patterson functions of the quasicrystal[19] and the associated hypercrystal,[18,20–23] and by imbedding structures of related periodic crystals into the hypercrystal.[7,9,24,25] Once the locations of the hyperatoms are known, their symmetries can be easily determined and used to constrain the hyperatom shapes and the form of their Debye-Waller factors. The Patterson functions may often suggest more details about the hyperatom shapes. For example, for all icosahedral and decagonal quasicrystals for

which Patterson functions were evaluated, it is found that to a good approximation hyperatoms are "flat", that is, $\mathbf{s}(\mathbf{r}^\perp) \equiv 0$, in a particular coordinate system. We shall show in the next section that this approximation is also applicable to i-$Al_{0.570}Cu_{0.108}Li_{0.322}$.

Even after all symmetry constraints are applied, and the hyperatoms are assumed flat, additional restrictions must be made in order to model the hyperatom shapes using a finite number of parameters. A restriction to ellipsoidal hyperatoms (i.e., ellipsoidal $v_\mu^\perp$), which is sometimes used,[18,24] allows for a finite parametrization (e.g., by positive symmetric quadratic forms). However, using such simple hyperatoms, it is impossible to simultaneously assure that the model density is correct *and* that the minimal interatomic separations are not violated. Consequently, more complicated hyperatoms emerge naturally, for example, by eliminating portions of the elliptical hyperatoms that cause too short interatomic distances.[18] Implementation of the restrictions on the interatomic separations may be simplified by assuming polytope shapes for the hyperatoms,[26,27] but this still requires a rather complex analysis. A great progress has been made recently for several quasicrystals using polytope modeling of the hyperatoms.[9,28] We shall further discuss this difficult subject elsewhere.[11]

We are concerned here with the solution of a more modest problem, that of reconstructing the phases and absolute scales of the structure factors at scattering wave vectors at which diffraction intensities are experimentally measured. In order to solve this problem, precise information about the hyperatom shapes is not necessary. We shall consider the case where the components $\mathbf{Q}^\perp$ of $\bar{\mathbf{Q}}$ fill the inner reciprocal space densely, and where the hyperatoms are sufficiently "nice" manifolds so that the inner-space atomic form factor $f_\mu^\perp(\mathbf{Q},\mathbf{Q}^\perp)$ defined by Eq. (A4) is an analytic function of two *continuous* variables, $\mathbf{Q}$ and $\mathbf{Q}^\perp$. In particular, we shall consider flat hyperatoms, $\mathbf{s}(\mathbf{r}^\perp) \equiv 0$, so that $f_\mu^\perp$ can be considered a (continuous) function of $\mathbf{Q}^\perp$ only. Therefore, we can represent $f_\mu^\perp(\mathbf{Q}^\perp)$ by an expansion into some basis functions with the expansion coefficients treated as fitting parameters. For example, we shall approximate $f_\mu^\perp(\mathbf{Q}^\perp)$ by its truncated Taylor series expansion,[29]

$$f_\mu^\perp(\mathbf{Q}^\perp) = \sum_l \left[\sum_{i_1}\sum_{i_2}\cdots\sum_{i_l}\right] f_{\mu i_1 i_2\cdots i_l}^{\perp(l)} Q_{i_1}^\perp Q_{i_2}^\perp \cdots Q_{i_l}^\perp. \tag{2.2}$$

The expansion coefficients $f_{\mu i_1 i_2\cdots i_l}^{\perp(l)}$ can be explicitly related to the hyperatom shape using Eqs. (2.2) and (A4),

$$\begin{aligned} f_{\mu i_1 i_2\cdots i_l}^{\perp(l)} &= \frac{(i)^l}{l!}\frac{1}{v_\mu^\perp}\int_{v_\mu^\perp} x_{i_1}^\perp x_{i_2}^\perp \cdots x_{i_l}^\perp dv^\perp \\ &\equiv \frac{(i)^l}{l!}\langle x_{i_1}^\perp x_{i_2}^\perp \cdots x_{i_l}^\perp\rangle_\mu, \end{aligned} \tag{2.3}$$

and the expansion can be expected to converge at least for $Q^\perp l_\mu^\perp \le 1$, where $l_\mu^\perp \sim (v_\mu^\perp)^{1/(D-3)}$ is the characteristic scale of the hyperatom. In particular, $f_\mu^{\perp(0)} \equiv 1$ by definition.

The expansion coefficients $f_{\mu i_1 i_2\cdots i_l}^{\perp(l)}$, properly constrained by the symmetry of the hyperatom, together with the densities n_μ, compositions $p_{\mu i}$, thermal ellipsoids $\bar{\mathsf{B}}_\mu$, and the scale s, can be treated as the fitting parameters in Eq. (2.1). However, it is clear that the inner-space Debye-Waller factor $e^{-\mathbf{Q}^\perp\cdot\mathsf{B}_\mu^\perp\cdot\mathbf{Q}^\perp}$ cannot be separated from $f_\mu^\perp(\mathbf{Q}^\perp)$ without some additional information, so that in practice we must use the expansion

$$\begin{aligned} &f_\mu^\perp(\mathbf{Q}^\perp)e^{-\mathbf{Q}^\perp\cdot\mathsf{B}_\mu^\perp\cdot\mathbf{Q}^\perp} \\ &\quad = \sum_l \left[\sum_{i_1}\sum_{i_2}\cdots\sum_{i_l}\right] c_{\mu i_1 i_2\cdots i_l}^{(l)} Q_{i_1}^\perp Q_{i_2}^\perp \cdots Q_{i_l}^\perp, \end{aligned} \tag{2.4}$$

in place of Eq. (2.2).

Furthermore, it can be seen from Eq. (A10) that if the atomic form factors $f_i(\mathbf{Q})$ are not sufficiently strong functions of the scattering vector $\mathbf{Q}$, it may not be possible to determine *independently* by the fit all the densities n_μ, compositions $p_{\mu i}$, and the scale s. For example, this occurs in the case of the neutron scattering where the neutron scattering lengths f_i are constants. Then, it follows from Eq. (A10) that only the combinations $g_\mu \equiv s^{-1}n_\mu f_\mu$ of these parameters can be determined (up to an overall arbitrary phase) directly by the fit Eq. (2.1). Therefore, if there are M independent hyperatoms and L chemical species, there are ML unknown $p_{\mu i}$'s, M unknown n_μ's, and the single unknown s. Once g_μ's are determined, this total of $M(L+1)+1$ unknowns is constrained by M equations

$$s^{-1}n_\mu \sum_i p_{\mu i} f_i = g_\mu, \tag{2.5}$$

which together with the M constraints provided by Eq. (A7) and another L constraints provided by Eq. (A8) give the total of $2M + L$ constraints. They are generally insufficient to fix all of the parameters and at least $(L-1)(M-1)$ parameters must remain undetermined by the fit. In fact, only when $M = 1$ or $L = 1$ the constraints are sufficient to uniquely solve for all of the parameters. Generally, the scale s and its arbitrary phase can be fixed,

$$s = \left|\sum_i n_i f_i \Big/ \sum_\mu g_\mu\right|, \tag{2.6}$$

and eliminated from Eq. (2.5),

$$n_\mu \sum_i p_{\mu i} f_i = g_\mu \frac{\sum_i n_i f_i}{\sum_\mu g_\mu}, \tag{2.7}$$

but one must remember that the number of independent equations is thus reduced by 1.

Clearly, the phase reconstruction depends crucially on the assumed truncation of the expansion and on the number of diffraction peaks $I_\mathbf{Q}$ measured in the experiment. With a larger number of diffraction peaks measured, it is possible to keep higher order terms in the Taylor expansion and thus calculate the structure factors with a

better accuracy. On the other hand, if the number of fitting parameters becomes comparable with the number of measured intensities, any phase reconstruction would result in an equally good fit. Thus, in order to evaluate the goodness of the fit, besides the residual factor R_F calculated as it is usually done in crystallography,

$$R_F = \frac{\sum_{\mathbf{Q}} \left| \sqrt{I_{\mathbf{Q}}} - \left| \frac{1}{s} F_{\mathbf{Q}} \right| \right|}{\sum_{\mathbf{Q}} \sqrt{I_{\mathbf{Q}}}}, \tag{2.8}$$

one should also consider statistical tests, such as the χ^2 test.

Even though some of the hyperatom parameters may remain undetermined, the absolute scale and the phases of the structure factors are completely determined and the reconstructed structure factor can be easily calculated:

$$F_{\mathbf{Q}}^{\mathrm{rec}} = s\sqrt{I_{\mathbf{Q}}} e^{i \arg(F_{\mathbf{Q}})}. \tag{2.9}$$

Moreover, the approximate structure factor $F_{\mathbf{Q}}$, calculated with the parametrization described above, can be used to interpolate the experimental data to the scattering vectors which were not experimentally accessible. Finally, combinations of the hyperatom parameters that *can* be determined by our method provide useful constraints for any subsequent structural modeling of the quasicrystal.

III. STRUCTURE FACTOR OF i-$Al_{0.570}Cu_{0.108}Li_{0.322}$

In this section, we shall apply the above analysis to reconstruct the neutron scattering structure factor of icosahedral quasicrystal i-$Al_{0.570}Cu_{0.108}Li_{0.322}$. We believe that the idealization of i-$Al_{0.570}Cu_{0.108}Li_{0.322}$ by a quasiperiodic crystal should be useful even if it is only approximate. This conclusion is supported by the following experimental evidence. The i-$Al_{0.570}Cu_{0.108}Li_{0.322}$ diffraction peaks can be indexed to within 10^{-3} Å^{-1} using an icosahedral reciprocal lattice. At the same time, the diffraction peak widths are also on the order of 10^{-3} Å^{-1}.[18] Moreover, the associated quasiperiodic Patterson function is extremely simple when viewed in the hyperspace, which would not be expected if quasiperiodicity were a bad assumption.[18,22,23] With the coordinate convention described in Ref. 30, the hyperlattice is simple cubic with its axes parallel to the Cartesian basis $\hat{\mathbf{e}}_j$ ($j = 1, \ldots, 6$) and with the lattice constant $\bar{a} = 7.15$ Å. The hyperlattice is oriented relative to the physical space so that the Cartesian lattice axes ($\hat{\mathbf{e}}_j$) project into the six icosahedral fivefold symmetry axes ($\hat{\mathbf{e}}_j$). Similarly, they project into the six icosahedral fivefold symmetry axes in the inner space ($\hat{\mathbf{e}}_j^{\perp}$).

An analysis of the Patterson function in the two-, three-, and fivefold hypercrystal symmetry planes, which contain the highest symmetry Wickoff positions, is consistent with the $P53m$ spacegroup symmetry[31] and the hyperatoms located at the vertex, $\bar{\mathbf{r}}_V = 0$, edge centers, $\bar{\mathbf{r}}_{E_j} = \frac{\bar{a}}{2}\hat{\mathbf{e}}_j$ ($j = 1, \ldots, 6$), and at the body center, $\bar{\mathbf{r}}_B = \frac{\bar{a}}{2}\sum_{j=1}^{6} \hat{\mathbf{e}}_j$, of the hypercubic unit cell.[18,22,23,32] It also strongly supports the assumption that the hyperatoms are "flat," that is, $\mathbf{s}_{\mu}(\mathbf{r}^{\perp}) \equiv 0$, $\mu = V, E_j, B$, and that they are considerably extended in the inner space. Thus, following Eq. (A1), we can write the structure factor of the icosahedral quasicrystal i-$Al_{0.570}Cu_{0.108}Li_{0.322}$ as

$$F_{\mathbf{Q}} = F_V(\bar{\mathbf{Q}}) + \sum_{j=1}^{6} (-1)^{m_j} F_{E_j}(\bar{\mathbf{Q}}) + (-1)^{\sum_j m_j} F_B(\bar{\mathbf{Q}}), \tag{3.1}$$

where $\bar{\mathbf{Q}} = \frac{2\pi}{\bar{a}} \sum_j m_j \hat{\mathbf{e}}_j$ and m's are the six Miller indices.

An indirect verification of the assumption that the hypercrystal consists of the vertex, midedge, and body-center hyperatoms can be seen in the branching of the diffraction data mentioned in the introduction and shown in Fig. 2(c). Indeed, as evident from Eq. (3.1), if we assume that all hyperatoms are nearly spherical, their physical space Debye-Waller factors approximately equal, say, $\exp(-BQ^2)$, and there are no off-diagonal physical–inner-space Debye-Waller factors, then the measured intensities, corrected for the physical space thermal motion, $I_{\mathbf{Q}}\exp(2BQ^2)$, should split depending on the number of even Miller indices into seven continuous functions of $Q^{\perp}$. More explicitly,

$$I_{\mathbf{Q}} e^{2BQ^2} \approx \left| g_V f_V^{\perp}(Q^{\perp}) e^{-B_V^{\perp} Q^{\perp 2}} + \left(\sum_{j=1}^{6} (-1)^{m_j} \right) g_E f_E^{\perp}(Q^{\perp}) e^{-B_E^{\perp} Q^{\perp 2}} + \left(\prod_{j=1}^{6} (-1)^{m_j} \right) g_B f_B^{\perp}(Q^{\perp}) e^{-B_B^{\perp} Q^{\perp 2}} \right|^2 \tag{3.2}$$

takes one of the seven values

$$I_0 = \left| g_V f_V^{\perp}(Q^{\perp}) e^{-B_V^{\perp} Q^{\perp 2}} - 6 g_E f_E^{\perp}(Q^{\perp}) e^{-B_E^{\perp} Q^{\perp 2}} + g_B f_B^{\perp}(Q^{\perp}) e^{-B_B^{\perp} Q^{\perp 2}} \right|^2, \tag{3.3}$$

$$I_1 = \left| g_V f_V^{\perp}(Q^{\perp}) e^{-B_V^{\perp} Q^{\perp 2}} - 4 g_E f_E^{\perp}(Q^{\perp}) e^{-B_E^{\perp} Q^{\perp 2}} - g_B f_B^{\perp}(Q^{\perp}) e^{-B_B^{\perp} Q^{\perp 2}} \right|^2, \tag{3.4}$$

$$I_2 = \left| g_V f_V^{\perp}(Q^{\perp}) e^{-B_V^{\perp} Q^{\perp 2}} - 2 g_E f_E^{\perp}(Q^{\perp}) e^{-B_E^{\perp} Q^{\perp 2}} + g_B f_B^{\perp}(Q^{\perp}) e^{-B_B^{\perp} Q^{\perp 2}} \right|^2, \tag{3.5}$$

$$I_3 = \left| g_V f_V^{\perp}(Q^{\perp}) e^{-B_V^{\perp} Q^{\perp 2}} - g_B f_B^{\perp}(Q^{\perp}) e^{-B_B^{\perp} Q^{\perp 2}} \right|^2, \tag{3.6}$$

$$I_4 = \left| g_V f_V^{\perp}(Q^{\perp}) e^{-B_V^{\perp} Q^{\perp 2}} + 2 g_E f_E^{\perp}(Q^{\perp}) e^{-B_E^{\perp} Q^{\perp 2}} + g_B f_B^{\perp}(Q^{\perp}) e^{-B_B^{\perp} Q^{\perp 2}} \right|^2, \tag{3.7}$$

$$I_5 = \left| g_V f_V^{\perp}(Q^{\perp}) e^{-B_V^{\perp} Q^{\perp 2}} + 4 g_E f_E^{\perp}(Q^{\perp}) e^{-B_E^{\perp} Q^{\perp 2}} - g_B f_B^{\perp}(Q^{\perp}) e^{-B_B^{\perp} Q^{\perp 2}} \right|^2, \tag{3.8}$$

$$I_6 = \left| g_V f_V^{\perp}(Q^{\perp}) e^{-B_V^{\perp} Q^{\perp 2}} + 6 g_E f_E^{\perp}(Q^{\perp}) e^{-B_E^{\perp} Q^{\perp 2}} + g_B f_B^{\perp}(Q^{\perp}) e^{-B_B^{\perp} Q^{\perp 2}} \right|^2. \tag{3.9}$$

Therefore, every diffraction peak of i-$Al_{0.570}Cu_{0.108}Li_{0.322}$ should fall into one of these seven branches. This is indeed the case in Fig. 2(c) where we used the value $B = 0.012$ Å^2 taken from our previous work.[7] This value is consistent with the typical values found in related crystals of known structure. Although the data set we use is not sufficiently large to clearly demonstrate this, the resulting branching should generally deteriorate for larger $Q^\perp$, because the hyperatoms are not exactly spherical, as well as for very small $Q^\perp$, where the largest Q's can be observed and, thus, the differences between the physical Debye-Waller factors of different hyperatoms are the largest.

As a parenthetical remark, one can also observe in Fig. 2(c) that for small $Q^\perp$ there is an approximate overalp of the pairs of branches,

$$\sqrt{I_2} - \sqrt{I_1} \approx \sqrt{I_3} - \sqrt{I_4} \approx \sqrt{I_5} - \sqrt{I_6} \approx 0, \quad (3.10)$$

implying that either $g_B \approx -g_E$ or $g_V \approx 3g_E$. However, the approximate relationships

$$\begin{aligned}\sqrt{I_0} - \sqrt{I_2} &\approx \sqrt{I_1} + \sqrt{I_3} \approx \sqrt{I_2} + \sqrt{I_4} \\ &\approx \sqrt{I_5} - \sqrt{I_3} \approx \sqrt{I_6} - \sqrt{I_4}, \end{aligned} \quad (3.11)$$

which can be also seen in the figure, eliminate $g_V \approx 3g_E$ because it would also imply $I_0 \approx I_3 \approx 0$, which is clearly not the case in the figure. These observations alone permit correct determination of the relative phases of the seven branches of structure factors for small $Q^\perp$: F_0 through F_2 have identical signs, opposite from the signs of F_3 through F_6, as shown in Fig. 2(d). This conclusion is confirmed below by our explicit calculation.

We now turn to the explicit parametrization of the three types of hyperatoms. The symmetry of the vertex and the body-center hyperatoms is Y_h and, as a consequence, their thermal tensors $\bar{\mathrm{B}}$ split into the physical and the inner space *scalar* components B and $B^\perp$. As explained earlier, the inner-space Debye-Waller factor is included into the expansion Eq. (2.4) which is limited here to fourth order in $Q^\perp$. The expansion simplifies due to Y_h symmetry and Eq. (A10) takes the form

$$F_V(\bar{\mathbf{Q}}) = n_V f_V \left[1 + \frac{1}{2}c_V^{(2)}Q^{\perp 2} + \frac{1}{4}c_V^{(2)}Q^{\perp 4}\right] e^{-B_V Q^2} \quad (3.12)$$

and

$$F_B(\bar{\mathbf{Q}}) = n_B f_B \left[1 + \frac{1}{2}c_B^{(2)}Q^{\perp 2} + \frac{1}{4}c_B^{(4)}Q^{\perp 4}\right] e^{-B_B Q^2}. \quad (3.13)$$

Each edge-center hyperatom has a D_{5d} symmetry that has to be manifested in the forms of both its thermal tensor and expansion of its structure factor. Therefore, the physical space thermal tensor splits into two scalar components, one longitudinal (B_{El}) and the other transverse (B_{Et}) to its fivefold symmetry axis coincident with an edge direction $\hat{\mathbf{e}}_j$. The inner-space thermal tensor, which will be included in the expansion Eq. (2.4), splits similarly with respect to the inner-space edge direction $\hat{\mathbf{e}}_j^\perp$. Although, unlike the Y_h symmetry, the D_{5d} symmetry does not eliminate the physical inner-space cross term of the thermal tensor, it forces it to have only a single, longitudinal-longitudinal, component B_{El}^x. The expansion Eq. (2.4) also simplifies due to the D_{5d} symmetry and Eq. (A10) takes the form

$$\begin{aligned} F_{E_j}(\bar{\mathbf{Q}}) = n_E f_E \Big[& 1 + \frac{1}{2}\left[c_{El}^{(2)}(\hat{\mathbf{e}}_j^\perp \cdot \mathbf{Q}^\perp)^2 + c_{Et}^{(2)}\left\{Q^{\perp 2} - (\hat{\mathbf{e}}_j^\perp \cdot \mathbf{Q}^\perp)^2\right\}\right] \\ & + \frac{1}{4}\left[c_{El}^{(4)}(\hat{\mathbf{e}}_j^\perp \cdot \mathbf{Q}^\perp)^4 + 2c_{Elt}^{(4)}(\hat{\mathbf{e}}_j^\perp \cdot \mathbf{Q}^\perp)^2\left\{Q^{\perp 2} - (\hat{\mathbf{e}}_j^\perp \cdot \mathbf{Q}^\perp)^2\right\} + c_{Et}^{(4)}\left\{Q^{\perp 2} - (\hat{\mathbf{e}}_j^\perp \cdot \mathbf{Q}^\perp)^2\right\}^2\right] \\ & \times e^{-\left[2B_{El}^x(\hat{\mathbf{e}}_j \cdot \mathbf{Q})(\hat{\mathbf{e}}_j^\perp \cdot \mathbf{Q}^\perp) + B_{El}(\hat{\mathbf{e}}_j \cdot \mathbf{Q})^2 + B_{Et}\left\{Q^2 - (\hat{\mathbf{e}}_j \cdot \mathbf{Q})^2\right\}\right]}. \end{aligned} \quad (3.14)$$

All the edge-center parameters are independent of a particular edge direction (that is, of j) because of the overall Y_h symmetry of the structure (for example, $n_{E_j} \equiv n_E$, $j = 1, \ldots, 6$).

In our calculation, we shall use the neutron diffraction data from Boissieu *et al.*,[18] where 40 reflections were measured. Since the atomic form factors f_i are independent of $\mathbf{Q}$ for neutron scattering, the hyperatom form factors $f_\mu = \sum_i p_{\mu i} f_i$ are also independent of $\mathbf{Q}$. Therefore, as mentioned in the previous section, it is not possible to fix all the chemical compositions $p_{\mu i}$ of the hyperatoms by fitting the neutron scattering data alone. The fitting procedure described in Eq. (2.1) allows us to determine the following 17 fitting parameters: (g_V, g_E, g_B), ($c_V^{(2)}$, $c_{El}^{(2)}$, $c_{Et}^{(2)}$, $c_B^{(2)}$), ($c_V^{(4)}$, $c_{El}^{(4)}$, $c_{Et}^{(4)}$, $c_{Elt}^{(4)}$, $c_B^{(4)}$), and (B_V, B_{El}, B_{Et}, B_{El}^x, B_B). The results of the fit are listed in Table I. They correspond to a small residual factor of $R_F = 0.051$, but the reduced χ^2 is somewhat worse ($\chi_\nu^2 = 2.47$) because of the relatively low ratio of the number of constraints (40) to the number of fitting parameters (17). The phases and the absolute scale of the total structure factor, as well as the structure factors of each hyperatom, can now be calculated using the parameters listed in Table I.

IV. DISCUSSION

With the parameters given in Table I, we first calculate the overall absolute scale using Eq. (2.6),

$$s = \left|\frac{n_{\mathrm{Al}} f_{\mathrm{Al}} + n_{\mathrm{Cu}} f_{\mathrm{Cu}} + n_{\mathrm{Li}} f_{\mathrm{Li}}}{g_V + 6g_E + g_B}\right| = 7.1(5) \times 10^{-8}\ \text{Å}^{-2} \quad (4.1)$$

TABLE I. The 17 fitting parameters obtained from the least-squares optimization of Eq. (2.1).

	V	E	B
g	5.1(3)	2.6(2)	-2.5(7)
B [Å^2]	0.011(1)	l: 0.013(2)	0.008(5)
		t: 0.0117(9)	
		x: 0.05(3)	
$c^{(2)}$ [Å^2]	-8.2(4)	l: −2(1)	-9(1)
		t: −8.2(3)	
$c^{(4)}$ [Å^4]	19(2)	l: −10(4)	19(4)
		t: 20(1)	
		lt: 15(2)	

where the neutron scattering lengths for the three chemical species are $f_{\rm Al} = 0.3449 \times 10^{-4}$ Å, $f_{\rm Li} = -0.203 \times 10^{-4}$ Å, and $f_{\rm Cu} = 0.7718 \times 10^{-4}$ Å, while their number densities, derived from the measured mass density of 2.47 g/cm^3 and chemical composition of i-$Al_{0.570}Cu_{0.108}Li_{0.322}$, are $n_{\rm Al} = 3.451 \times 10^{-2}$ Å^{-3}, $n_{\rm Cu} = 6.541 \times 10^{-3}$ Å^{-3}, and $n_{\rm Li} = 1.950 \times 10^{-2}$ Å^{-3}. Next, we calculate the right-hand side of Eq. (2.7), $n_V f_V = 0.36(3) \times 10^{-6}$ Å^{-2}, $n_E f_E = 0.19(2) \times 10^{-6}$ Å^{-2}, and $n_B f_B = -0.18(5) \times 10^{-6}$ Å^{-2}. Finally, we calculate the approximate and the reconstructed structure factors using Eqs. (3.1, 3.12–3.14) and Eq. (2.9), respectively. In Fig. 2(d) we plotted the experimentally observed magnitude of the structure factors (in arbitrary units) $\sqrt{I_{\mathbf{Q}}}$, multiplied by the obtained phase factors $\exp[i \arg(F_{\mathbf{Q}})] = \pm 1$.

The structure factors reconstructed in this paper are in a good agreement with the ones reconstructed earlier using a different, rational approximant, method.[7] This can be clearly seen from Fig. 4 where we show the approximate structure factor determined here plotted versus the reconstructed structure factor determined in Ref. 7. All the phases are in agreement except for the two associated with the weak intensities. They correspond to the only two points in Fig. 4 that are in the second quadrant of the figure. In Fig. 2(d), these are the two points with the largest $Q^\perp$ among the ponts with three even Miller indices [$(2221\bar{1}1)$ and (333002)]. All the points in Fig. 4 fall around a straight line through the origin inclined at approximately ±45°, indicating that the absolute scales are consistent. Indeed, the scales found here and in Ref. 7 are $7.1(5) \times 10^{-8}$ Å^{-2} and $7.4(1) \times 10^{-8}$ Å^{-2}, respectively. Smallness of the data scatter around the straight line reflects the high quality of the fit accomplished with the parametrization described here. Finally, thermal fluctuations of atoms calculated in this paper [$B_V = 0.011(1)$ Å^2, $B_{El} = 0.013(2)$ Å^2, $B_{Et} = 0.0117(9)$ Å^2, and $B_B = 0.008(5)$ Å^2] are also comparable to the result of the earlier rational approximant method,[7] where only an overall Debye-Waller factor could be obtained [$B = 0.0120(3)$ Å^2].[33]

Although the inner-space Debye-Waller factors cannot be separated from the inner-space atomic form factors, ideally, they can be constrained by the expansion coefficients in Eq. (2.4). For example, to second order $c^{(2)}_{\mu i_1 i_2}$ equals $f^{\perp(2)}_{\mu i_1 i_2} - B^\perp_{\mu i_1 i_2}$, and we can use positivity of the quadratic form $\langle x^\perp_{i_1} x^\perp_{i_2} \rangle$ to obtain the matrix inequality

$$\mathsf{B}^\perp_\mu + \mathsf{c}^{(2)} < 0. \tag{4.2}$$

Similar tensor inequalities can be derived from the higher order terms. However, these inequalities are exact only for an infinite expansion. In practice, they must be considered only approximate since the coefficients $\mathsf{c}^{(l)}_\mu$ are determined from a truncated expansion and are, thus, approximate. The approximation is best for lower order terms and it improves with increased order of the truncation.

In particular, the second order terms with Y_h symmetry are constrained by $\langle r^{\perp 2} \rangle > 0$ giving the approximate upper bounds $B^\perp_V < -\frac{1}{2} c^{(2)}_V = 4.11(3)$ Å^2 and $B^\perp_B < -\frac{1}{2} c^{(2)}_B = 4.74(8)$ Å^2. The second order terms with D_{5d} symmetry are constrained by $\langle r^{\perp 2}_t \rangle > 0$ and $\langle r^{\perp 2}_l \rangle > 0$ which lead to the approximate upper bounds $B^\perp_{Et} < -\frac{1}{2} c^{(2)}_{Et} = 4.12(2)$ Å^2 and $B^\perp_{El} < -\frac{1}{2} c^{(2)}_{El} = 1.16(7)$ Å^2. The value obtained in Ref. 7 for an overall inner-space Debye-Waller factor, $B^\perp = 0.39(7)$ Å^2, is consistent with these upper bounds. Moreover, it is also consistent with the lower bound $B^\perp_{El} > (B^x_{El})^2 / B_{El} = 0.2(2)$ Å^2 which assures positivity of the thermal tensor $\bar{\mathsf{B}}_E$. Although most of the more stringent constraints resulting from the fourth order terms are also consistent with the above value for $B^\perp$, they are the least reliable since we truncated the expansion Eq. (2.4) at the fourth order.[34]

As we already mentioned, the scale s, the chemical compositions $p_{\mu i}$, and the physical space densities n_μ of the hyperatoms cannot be all determined by the fit. They constitute here the total of 13 parameters, connected by the total of nine constraints, three resulting from each of the Eqs. (2.7), (A7), and (A8). Thus, at the most nine parameters can be independently fixed. In order to fix the remaining four parameters, more constraints must be obtained from additional independent assumptions. For example, a consideration of the crystalline R-$Al_{0.564}Cu_{0.116}Li_{0.320}$, which is believed to be a rational approximant of i-$Al_{0.570}Cu_{0.108}Li_{0.322}$, can provide appropriate constraints. When R-$Al_{0.564}Cu_{0.116}Li_{0.320}$ is embedded in the six-dimensional hypercrystal, all the Li atoms and some Al atoms, but no Cu atoms, are located near the body center of the hypercell.[25,7] If we assume that the same compositional constraints apply to the entire hyperatoms, we obtain three new constraints, $p_{B\rm Cu} = 0$, $p_{V\rm Li} = 0$, and $p_{E\rm Li} = 0$, and only one free parameter remains, say, $p_{V\rm Cu}/p_{E\rm Cu}$. These constraints, combined with Eqs. (2.7,A7,A8) are sufficient to completely specify the body-center hyperatom, giving $n_B = 2.6(1) \times 10^{-2}$ Å^{-3}, $p_{B\rm Li} = 0.75(4)$, and $p_{B\rm Al} = 0.25(4)$. This information is most useful for the modeling when translated into the body-center hyperatom volume $v^\perp{}_B = 3.5(2) \times 10^3$ Å^3 and the volumes $v^\perp{}_{B\rm Li} = 2.605 \times 10^3$ Å^3 and $v^\perp{}_{B\rm Al} = 0.9(2) \times 10^3$ Å^3 of its Li and Al portions, respectively.[11]

In the above example one might try to simplify the analysis by neglecting any Al on the body-center hyperatom. This would add the fourth constraint, $p_{B\rm Al} = 0$, seemingly fixing all the parameters. However, this con-

straint is no longer independent because we could now determine the scale s not only by Eq. (2.6) [$s = 7.1(5) \times 10^{-8}$ Å^{-2}] but also with $s = |n_{\mathrm{Li}} f_{\mathrm{Li}}/g_B| = 16(4) \times 10^{-8}$ Å^{-2} or $s = |(n_{\mathrm{Al}} f_{\mathrm{Al}} + n_{\mathrm{Cu}} f_{\mathrm{Cu}})/(g_V + 6g_E)| = 8.2(4) \times 10^{-8}$ Å^{-2}, which are obviously mutually inconsistent in this case. Conversely, we may use this information to infer that some mixing of Li with Al or Cu must occur within hyperatoms.

The approximate, parametrized structure factor can be also used to help modeling of the atomic structure of the quasicrystal.[11] As already mentioned, since it is an explicit function of the quasicrystal scattering wave vector, the approximate structure factor can be used to effectively enlarge the "diffraction data" set and interpolate the structure factors at the values of experimentally inaccessible wave vectors. In this way, the truncated Fourier series [Eq. (1.1)] can be extended to give more accurately the (hyperspace) density of scatterers. Moreover, since this method actually gives parametrized structure factors of individual hyperatoms, which are continuous functions of the inner-space scattering wave vector, it allows for a more meaningful interpolation as well as some extrapolation of the data. This, in turn, facilitates more accurate determination of the inner-space density of individual hyperatoms. The hyperatoms are smeared into continuous densities by the inner-space fluctuations, which we cannot isolate and remove within this method. However, since the physical space Debye-Waller factors are determined by this method, the physical space fluctuations can be removed from the structure factors, considerably sharpening the density and, thus, providing useful guidance in the modeling of the hyperatom shapes.

Further analysis of the hyperatom densities and of the consequences of our results on the modeling of i-$Al_{0.570}Cu_{0.108}Li_{0.322}$ will be presented elsewhere.[10,11] Here we only mention some obvious limitations. Because of the relatively small data set we had available here, we restricted our parametrization of the hyperatom structure factors to only fourth degree in $Q^{\perp}$. In order to reveal the true symmetry of the hyperatoms it is necessary to carry out the expansion to at least sixth order. This can be done with a larger x-ray data set[18] which also provides more stringent constraints on the hyperatom compositions. It is very important to emphasize that the most severe limitation on the use of our results to help structure modeling stems from the inevitable truncation of the experimental data and, consequently, inaccurate reconstruction of the scatterer densities. This problem can be partially alleviated by a judicial choice of the functional basis for the expansion to allow for a significant *extrapolation* of the data set. However, this is precisely where the borderline between structure modeling and structure factor reconstruction begins to blur.

V. CONCLUSION

In this paper, we showed how the inner-space structure factors of hyperatoms can be approximately parametrized and the parameters fitted using the experimentally measured diffraction intensities of quasiperiodic crystals. We thereby also presented a method for the reconstruction of the absolute scale and phases of structure factors of quasiperiodic crystals, a method which complements a different reconstruction method based on periodic approximants of quasiperiodic crystals.[7] Although the two methods are based on significantly different sets of assumptions, we demonstrated on the example of i-$Al_{0.570}Cu_{0.108}Li_{0.322}$ neutron structure factors that they yield consistent results: All 40 phases, except for two that are associated with weak peaks, are consistent, and the absolute scales and the physical space Debye-Waller factors are within the error bars. The parametrization we used appears adequate as attested by the very good residual factor R_F=0.051. We have also discussed to what extent the results of the reconstruction can be used to guide structure modeling, and we briefly considered i-$Al_{0.570}Cu_{0.108}Li_{0.322}$. A more detailed analysis of the results of reconstruction and of the structure modeling of i-$Al_{0.570}Cu_{0.108}Li_{0.322}$ requires a separate publication.[10,11] We conclude that the method we presented here can be particularly useful in cases where periodic approximants of a given quasicrystal are not known. On the other hand, even when periodic approximants are known, this method can be easily combined with the rational approximant method by parametrizing the hyperatom structure factors as described here and then applying the rational approximant method to each hyperatom type. This could yield more accurate information about the hyperatom structure factors. It is left for a future investigation to formally integrate these two approaches into a single more powerful method.

Note added in proof. Inconsistent values are reported in the literature for the mass densities or isotope content of i-$Al_{0.570}Cu_{0.108}Li_{0.322}$ and R-$Al_{0.564}Cu_{0.116}Li_{0.320}$ samples used here and in Ref. 7. However, this variation does not affect our results significantly.[11]

ACKNOWLEDGMENTS

One of us (M.V.J.) is grateful to colleagues at the University of California Santa Cruz for hospitality. This research was supported in part by the NSF Grants Nos. DMR8821802 and DMR9215231.

APPENDIX: STRUCTURE FACTOR OF QUASICRYSTALS

As is well known, a quasiperiodic crystal can be viewed as a cut through a higher dimensional periodic crystal (hypercrystal). The quasiperiodicity dictates that the cut is not parallel to any of the crystallographic planes of the hypercrystal. This implies a one-to-one correspondence between the reciprocal lattice vectors $\bar{\mathbf{Q}} = (\mathbf{Q}, \mathbf{Q}^{\perp})$ and $\mathbf{Q}$ of the hypercrystal and quasicrystal, respectively. By definition, the hypercrystal structure factor $\bar{F}_{\bar{\mathbf{Q}}}$ is equal, up to an overall phase factor, to the quasicrystal structure factor $F_{\mathbf{Q}}$. (Hereafter, all quantities with an overbar are distinguished as hyperspace quantities, while quantities with a $\perp$ superscript are associated with the "inner space," the orthogonal complement to the physical space.) On the other hand, since the hypercrystal is periodic, its structure factor is given by a straightforward generalization of the usual formula for periodic crystals. Therefore,

$$F_{\mathbf{Q}} \equiv \bar{F}_{\bar{\mathbf{Q}}} = \sum_{\mu} F_{\mu}(\bar{\mathbf{Q}}) e^{i\bar{\mathbf{Q}}\cdot\bar{\mathbf{r}}_{\mu}}, \tag{A1}$$

where the sum is over all *hyperatoms* within the unit hypercell, $\bar{\mathbf{r}}_{\mu}$ is the location of the μth hyperatom in the unit cell, and $F_{\mu}(\bar{\mathbf{Q}})$ its contribution.

If the cut through the hypercrystal is to produce point-like atoms in the three-dimensional physical space, the hyperatoms must be extended objects of codimension 3. Therefore, a hyperatom must be characterized not only by its chemical character, but also by its geometrical "shape,"

$$\mathbf{r} = \mathbf{s}_{\mu}(\mathbf{r}^{\perp}), \qquad \mathbf{r}^{\perp} \in v_{\mu}^{\perp}, \tag{A2}$$

which requires specifying the function $\mathbf{s}_{\mu}(\mathbf{r}^{\perp})$ as well as the shape of the inner-space domain $v_{\mu}^{\perp}$. The volume of this domain, which we shall also denote by $v_{\mu}^{\perp}$, determines the number density n_{μ} of the corresponding atoms in the physical space,

$$n_{\mu} = \frac{v_{\mu}^{\perp}}{\bar{v}}, \tag{A3}$$

where $\bar{v}$ is the volume of the unit hypercell. The hyperatom shape contributes a factor $n_{\mu} f_{\mu}^{\perp}(\bar{\mathbf{Q}})$ to $F_{\mu}(\bar{\mathbf{Q}})$, where $f_{\mu}^{\perp}(\bar{\mathbf{Q}})$, the inner-space atomic form factor, is the inner-space Fourier transform of the hyperatom,

$$f_{\mu}^{\perp}(\bar{\mathbf{Q}}) = \frac{1}{v_{\mu}^{\perp}} \int_{v_{\mu}^{\perp}} e^{i\mathbf{Q}^{\perp}\cdot\mathbf{r}^{\perp}} e^{i\mathbf{Q}\cdot\mathbf{s}_{\mu}(\mathbf{r}^{\perp})} dv^{\perp}. \tag{A4}$$

In addition to the inner-space form factor, $F_{\mu}(\bar{\mathbf{Q}})$ also contains the usual physical space atomic form factor $f_{\mu}(\mathbf{Q})$. It can be expressed in terms of the atomic form factors $f_i(\mathbf{Q})$ of the chemical species i that compose the hyperatom,

$$f_{\mu}(\mathbf{Q}) = \sum_{i} p_{\mu i} f_i(\mathbf{Q}), \tag{A5}$$

where $p_{\mu i}$ is the fraction of the chemical species i in the hyperatom μ. These fractions must satisfy the obvious relations

$$0 \le p_{\mu i} \le 1 \tag{A6}$$

and

$$\sum_{i} p_{\mu i} = 1, \tag{A7}$$

as well as the constraints imposed by the experimentally accessible number densities n_i of the chemical species in the quasiperiodic crystal itself,

$$\sum_{\mu} n_{\mu} p_{\mu i} = n_i. \tag{A8}$$

Finally, $F_{\mu}(\bar{\mathbf{Q}})$ contains a "Debye-Waller factor" $e^{-\bar{\mathbf{Q}}\cdot\bar{\mathbf{B}}_{\mu}\cdot\bar{\mathbf{Q}}}$ which results from disorder (thermal fluctuations) in the quasiperiodic crystal. The appearance of $\bar{\mathbf{Q}}$ rather than only $\mathbf{Q}$ in the exponent reflects the possible presence in quasiperiodic crystals of the "phason" fluctuations in addition to the usual phonon fluctuations. Putting all these factors together, we find

$$F_{\mu}(\bar{\mathbf{Q}}) = n_{\mu} f_{\mu}(\mathbf{Q}) f_{\mu}^{\perp}(\bar{\mathbf{Q}}) e^{-\bar{\mathbf{Q}}\cdot\bar{\mathbf{B}}_{\mu}\cdot\bar{\mathbf{Q}}}, \tag{A9}$$

and the quasicrystal structure factor can be written more explicitly as

$$F_{\mathbf{Q}} = \sum_{\mu} n_{\mu} f_{\mu}(\mathbf{Q}) f_{\mu}^{\perp}(\bar{\mathbf{Q}}) e^{i\bar{\mathbf{Q}}\cdot\bar{\mathbf{r}}_{\mu}} e^{-\bar{\mathbf{Q}}\cdot\bar{\mathbf{B}}_{\mu}\cdot\bar{\mathbf{Q}}}. \tag{A10}$$

[1] D. Levine and P. J. Steinhardt, Phys. Rev. Lett. **53**, 2477 (1984).

[2] P. A. Kalugin, A. Yu. Kitayev, and L. S. Levitov, Pis'ma Zh. Eksp. Teor. Fiz. **41**, 119 (1985) [JETP Lett. **41**, 145 (1985)].

[3] P. Bak, Phys. Rev. Lett. **54**, 1517 (1985).

[4] M. Duneau and A. Katz, Phys. Rev. Lett. **54**, 2688 (1985).

[5] V. Elser, Phys. Rev. B **32**, 4892 (1985).

[6] Therefore, quasicrystals are a special case of more general incommensurate crystals—they are distinguished by a non-crystallographic point-group symmetry.

[7] M. V. Jarić and S.-Y. Qiu, Acta Crystallogr. A **49**, 576 (1993).

[8] C. Janot, M. de Boissieu, and J.-M. Dubois, in *Quasicrystals*, edited by M. V. Jarić and S. Lundqvist (World Scientific, Singapore, 1989), p. 34.

[9] M. Cornier-Quiquandon, A. Quivy, S. Lefebvre, E. Elkain, G. Heger, A. Katz, and D. Gratias, Phys. Rev. B **44**, 2071 (1991).

[10] S.-Y. Qiu and M. V. Jarić (unpublished).

[11] S.-Y. Qiu and M. V. Jarić (unpublished).

[12] J. M. Dubois, C. Janot, and J. Pannetier, Phys. Lett. A **115**, 177 (1986).

[13] M. Boudard, M. de Boissieu, C. Janot, J. M. Dubois, and C. Dong, Philos. Mag. Lett. **64**, 197 (1991).

[14] M. Cornier-Quiquandon, R. Bellissent, Y. Calvayrac, J. W. Cahn, D. Gratias, and B. Mozer, J. Non-Cryst. Solids **153&154**, 10 (1993).

[15] H. Hauptman, Science **233**, 178 (1986).

[16] J. Karle, Science **232**, 837 (1986).

[17] C. Janot, J. M. Dubois, and M. de Boissieu, in *Proceedings of the NATO Advanced Research Workshop on Common Problems of Quasicrystals, Liquid Crystals and Incommensurate Insulators*, edited by J. C. Tolédano (Plenum, New York, 1990), p. 9.

[18] M. de Boissieu, C. Janot, J. M. Dubois, M. Audier, and B. Dubost, J. Phys. Condens. Matter **3**, 1 (1991).

[19] J. W. Cahn, D. Gratias, and B. Mozer, Phys. Rev. B **38**, 1638 (1988).

[20] J. W. Cahn, D. Gratias, and B. Mozer, Phys. Rev. B **38**, 1643 (1988).

[21] W. Steurer, Acta Crystallogr. B **45**, 534 (1989).

[22] S.-Y. Qiu and M. V. Jairć, in *Quasicrystals*, edited by M. V. Jarić and S. Lundqvist (World Scientific, Singapore, 1989), p. 19.

[23] S. van Smaalen, J. L. Boer, and Y. Shen, Phys. Rev. B **43**,

929 (1991).
[24] J. W. Cahn, D. Gratias, and B. Mozer, J. Phys. (Paris) **49**, 1225 (1988).
[25] A. Yamamoto, in *Quasicrystals*, edited by T. Fujiwara and T. Ogawa (Springer, Berlin, 1990), p. 57.
[26] M. Duneau and C. Oguey, J. Phys. (Paris) **50**, 135 (1989).
[27] M. Cornier-Quiquandon, D. Gratias, and A. Katz, in *Methods of Structural Analysis of Modulated Structures and Quasicrystals*, edited by J. M. Pérez-Mato, F. J. Zúñiga, and G. Madriaga (World Scientific, Singapore, 1991), p. 313.
[28] A. Yamamoto, Phys. Rev. B **45**, 5217 (1992).
[29] It is well known that the least-squares fit of a function to a truncated Taylor expansion becomes less stable as the degree of truncation is increased, so that improved accuracy of the fit may often require a different functional expansion.
[30] M. V. Jarić, J. Phys. (Paris) **47**, 82 (1986).
[31] D. Mermin, J. Mod. Phys. **64**, 3 (1992).
[32] H. B. Elswijk, J. Th. M. de Hosson, S. van Smaalen, and J. L. de Boer, Phys. Rev. B **38**, 1681 (1991).
[33] It is interesting to note that we found a local minimum in our least-squares minimization (χ^2_ν=2.91) at which all reconstructed phases are identical to these determined in Ref. 7, the reconstructed scale $7.5(4)\times10^{-8}$ Å^{-2} is nearly identical to the scale found there, and the thermal Debye-Waller factors are also comparable [B_V = 0.011(1) Å^2, B_{El} = 0.010(2) Å^2, B_{Et} = 0.0115(9) Å^2, and B_B = 0.004(4) Å^2]. The main differences between this local minimum and the global minimum are in the $c^{(4)}$ coefficients.
[34] The fourth order constraints $\langle r^{\perp 4}\rangle > 0$, for V and B hyperatoms, and $\langle r_l^{\perp 4}\rangle > 0$ and $\langle r_t^{\perp 4}\rangle > 0$, for E hyperatoms, are equivalent to a more stringent upper bound $B_\mu < \frac{1}{2}[-c_\mu^{(2)} - \sqrt{(c_\mu^{(2)})^2 - 2c_\mu^{(4)}}]$ which gives $B_V^\perp < 1.41(3)$ Å^2, $B_B^\perp < 1.15(5)$ Å^2, $B_{El}^\perp < 0.0(1)$ Å^2, and $B_{Et}^\perp < 1.44(2)$ Å^2. If $B_{El}^\perp$ and $B_{Et}^\perp$ were approximately equal, positivity of $\langle r_l^{\perp 2} r_t^{\perp 2}\rangle_E$ would reduce to the bound $B_{El}^\perp \approx B_{Et}^\perp < \frac{1}{2}[-c_{Elt}^{(2)} - \sqrt{(c_{Elt}^{(2)})^2 - 2c_{Elt}^{(4)}}] = 0.0(1)\times10^2$ Å^2, where $c_{Elt}^{(2)} \equiv \frac{1}{2}(c_{El}^{(2)} + c_{Et}^{(2)})$. These more stringent bounds are, surprisingly, still consistent with $B^\perp$ determined in Ref. 7. The constraint $\langle r^{\perp 4}\rangle > \langle r^{\perp 2}\rangle^2$ and similar ones for r_l and r_t yield still more stringent bounds, $B_\mu^\perp < \frac{1}{2}\{-c_\mu^{(2)} - \sqrt{k_\mu[(c_\mu^{(2)})^2 - 2c_\mu^{(4)}]}\}$, where $k_V = k_B = \frac{5}{2}$, $k_{Et} = 2$, and $k_{El} = \frac{3}{2}$. It produces $B_V^\perp < -0.15(6)$ Å^2, $B_B^\perp < -0.9(1)$ Å^2, $B_{El}^\perp < -0.3(2)$ Å^2, and $B_{Et}^\perp < 0.33(3)$ Å^2. Obviously, these bounds for V, B, and El are inconsistent with Ref. 7. They are also inconsistent with the positivity of the thermal tensors, emphasizing unreliability of the constraints derived from the terms close to the truncation of the structure-factor expansion.